Exploring the Many-Body Dynamics Near a Conical Intersection with Trapped Rydberg Ions

Filippo M. Gambetta,[1,2] Chi Zhang,[3] Markus Hennrich,[3] Igor Lesanovsky,[1,2,4] and Weibin Li[1,2]
[1]School of Physics and Astronomy, University of Nottingham, Nottingham, NG7 2RD, United Kingdom
[2]Centre for the Mathematics and Theoretical Physics of Quantum Non-equilibrium Systems, University of Nottingham, Nottingham NG7 2RD, United Kingdom
[3]Department of Physics, Stockholm University, 10691 Stockholm, Sweden
[4]Institut für Theoretische Physik, University of Tübingen, 72076 Tübingen, Germany

(Received 9 December 2020; revised 11 April 2021; accepted 12 May 2021; published 11 June 2021)

Conical intersections between electronic potential energy surfaces are paradigmatic for the study of nonadiabatic processes in the excited states of large molecules. However, since the corresponding dynamics occurs on a femtosecond timescale, their investigation remains challenging and requires ultrafast spectroscopy techniques. We demonstrate that trapped Rydberg ions are a platform to engineer conical intersections and to simulate their ensuing dynamics on larger length scales and timescales of the order of nanometers and microseconds, respectively; all this in a highly controllable system. Here, the shape of the potential energy surfaces and the position of the conical intersection can be tuned thanks to the interplay between the high polarizability and the strong dipolar exchange interactions of Rydberg ions. We study how the presence of a conical intersection affects both the nuclear and electronic dynamics demonstrating, in particular, how it results in the inhibition of the nuclear motion. These effects can be monitored in real time via a direct spectroscopic measurement of the electronic populations in a state-of-the-art experimental setup.

DOI: 10.1103/PhysRevLett.126.233404

Introduction.—The Born-Oppenheimer (BO) approximation is a cornerstone of modern solid state and molecular theories [1,2]. It provides a simple description of many electronic systems in which nuclei move on a single potential energy surface (PES) generated by the electronic dynamics. Nevertheless, nonadiabatic phenomena, which fall outside the validity regime of the BO approximation, are ubiquitous in many fundamental chemical processes [3]. Among them, conical intersections (CIs), which occur when two (or more) PESs are degenerate within a given submanifold of the nuclear coordinates, are at basis of many fundamental photochemical processes in large molecules [2,4,5]. They provide a fast and radiationless deexcitation mechanism between intramolecular electronic states [6,7], which contributes to the stability of DNA [8], to the mechanism of vision [9–11], and to photosynthesis [12]. Importantly, CIs are tightly linked to the emergence of geometric phase (GP) effects: during the motion on a path that encircles a CI, both the electronic and nuclear wave functions acquire an extra phase factor of π, which results in observable interference phenomena [13–19]. Despite the understanding of CIs developed over the past decades, passages through a CI in real time have been observed only recently [2,4,5,10,20]. Since processes associated with CIs occur typically on a femtosecond timescale, ultrafast and broadband spectroscopy techniques are indeed needed to record the features of dynamics they induce [21–24]. Moreover, the observation of GP effects requires a high degree of control on the preparation of the nuclear wave function, which is hardly achievable in real molecules. In recent years, ultracold gases have been proposed as a tool to overcome all of these issues and to study CIs in a well-controlled environment [25–27], with Rydberg atoms [28,29] suggested as a quantum simulator for the dynamics in the neighborhood of a CI [30,31].

In this work we show that trapped Rydberg ions offer ideal properties for controlling and investigating the quantum many-body dynamics near a CI. They combine the high degree of control typical of trapped ion setups with tunable dipole-dipole interactions, enabled by the possibility to individually excite each ion to a high-lying Rydberg level [32–41]. Moreover, due to the interplay between the state-dependent polarizability of Rydberg states and the radiofrequency electric field of the Paul trap, Rydberg ions feature a controllable state-dependent trapping potential [42,43]. We show that this mechanism, in the presence of two different Rydberg states and combined with strong dipolar exchange interactions between two Rydberg ions, can be exploited to realize a minimal instance of a CI, consisting of two electronic states and two nontrivial nuclear coordinates [2], shown in Fig. 1. The PESs and the position of the CI are controlled by the exchange interactions and an external electric field, allowing one to realize various scenarios which occur, e.g., in

photochemical processes, but on nanometer length and microsecond timescales. The high degree of control over the vibrational motion of the ions makes it possible to minimize decoherence effects stemming from the coupling to additional rovibrational nuclear degrees of freedom. The latter, which cannot be avoided in real molecules, affects the dynamics across a CI on a subpicosecond timescale and hinders the experimental observation of coherent quantum effects [44–46]. To demonstrate the capabilities of our approach, we investigate effects induced by the GP in a feasible experimental setup: We show that the destructive interference between the paths encircling the different sides of a CI results in the localization of the nuclear wave packet. This GP effect can be directly observed via a measurement of the electronic state population and does not require the spatially resolved detection of each ion.

Equations of motion.—We consider a system of two Rydberg ions of mass m in a linear Paul trap. The latter gives rise to an effective harmonic trapping potential with frequencies $\omega_{X,Y,Z}$ [42,43,47]. For the sake of simplicity, we assume $\omega_Y \gg \omega_X > \omega_Z$, so that the motion of the ions is confined to the X–Z plane, with the Z axis being the longitudinal one; see Fig. 1. The potential energy of the two trapped ions is $V_{\rm trap} = m[\omega_X^2(X_1^2+X_2^2)+\omega_Z^2(Z_1^2+Z_2^2)]/2 + ke^2/r$, where the last term corresponds to the repulsive Coulomb interaction [with $k = 1/(4\pi\epsilon_0)$ being the Coulomb constant]. Here, $\boldsymbol{r} = \boldsymbol{R}_1 - \boldsymbol{R}_2$, with $\boldsymbol{R}_i = (X_i, Z_i)$, $i \in \{1,2\}$, the nuclear coordinates in the laboratory frame. From their ground state $|g\rangle$, the ions can be excited to the two Rydberg levels $|nS\rangle = |\downarrow\rangle$ and $|nP\rangle = |\uparrow\rangle$, with n being the principal quantum number, both of which can be coupled by a microwave (MW) field with Rabi frequency Ω. Rydberg-excited ions interact via the exchange interaction potential $V_{\rm ex}(r)\cdot(\sigma_+^1\otimes\sigma_-^2+\sigma_-^1\otimes\sigma_+^2)$, with $\sigma_\pm^i$ acting on the ith ion as $\sigma_+^i|\downarrow^i\rangle = |\uparrow^i\rangle$ and $\sigma_-^i|\uparrow^i\rangle = |\downarrow^i\rangle$. Furthermore, due to the large polarizability of Rydberg levels (denoted by ρ_σ, with $\sigma \in \{\downarrow,\uparrow\}$), ions in the Rydberg states experience an additional transverse trapping potential $\delta V_{{\rm trap},\sigma} = -\rho_\sigma A^2(X_1^2+X_2^2)$, where A is the gradient of the radio-frequency field of the Paul trap [42,43]. Finally, the transverse equilibrium positions of the ions is controlled via a static offset electric field $\boldsymbol{\mathcal{E}}$ along the X axis, which results in the potential energy contribution $V_{\rm mm} = e\mathcal{E}(X_1+X_2)$. In what follows we will focus on the dynamics in the spin subspace $\mathcal{H}_{\rm sp}$, which is spanned by the ion pair states $|\pi_1\rangle = |\uparrow\downarrow\rangle$ and $|\pi_2\rangle = |\downarrow\uparrow\rangle$. The latter define the so-called *diabatic basis* of the system [30,31]. In this subspace, we define the Pauli operators $S_0 = |\pi_1\rangle\langle\pi_1| + |\pi_2\rangle\langle\pi_2|$, $S_x = |\pi_1\rangle\langle\pi_2| + |\pi_2\rangle\langle\pi_1|$, and $S_z = |\pi_1\rangle\langle\pi_1| - |\pi_2\rangle\langle\pi_2|$.

The system is most conveniently analyzed in the center of mass (c.m.) reference frame, with $\boldsymbol{R} = (X,Z) = (\boldsymbol{R}_1+\boldsymbol{R}_2)/2$ and $\boldsymbol{r} = (x,z)$ the c.m. and the relative coordinates, respectively. In terms of the latter, the full system Hamiltonian is

$$H = \left(-\frac{\nabla_{\boldsymbol{R}}^2}{2M} - \frac{\nabla_{\boldsymbol{r}}^2}{2\mu}\right)\otimes S_0 + H_{\rm spin}, \tag{1}$$

where the first term accounts for the total kinetic energy, with $M = 2m$ and $\mu = m/2$ the c.m. and reduced mass, respectively. The potential energy contributions are contained in $H_{\rm spin} = H_{\rm spin}^0 + H_{\rm spin}^1$, with

$$H_{\rm spin}^0 = (V_{\rm c.m.} + V_{\rm rel})\otimes S_0, \tag{2a}$$

$$H_{\rm spin}^1 = V_{\rm ex}(r)\otimes S_x + H_{\rm c.m.-rel}. \tag{2b}$$

Here, by defining the polarizabilities $\rho_\pm = \rho_\uparrow \pm \rho_\downarrow$, we have

$$V_{\rm c.m.} = \frac{M}{2}[\bar{\omega}_X^2(X-X^0)^2 + \omega_Z^2 Z^2], \tag{3a}$$

$$V_{\rm rel} = \frac{\mu}{2}(\bar{\omega}_X^2 x^2 + \omega_Z^2 z^2) + \frac{ke^2}{r}. \tag{3b}$$

Equation (3a) corresponds to a harmonic trapping potential with renormalized frequency $\bar{\omega}_X^2 = \omega_X^2 - A^2\rho_+/m$ and displaced along the x direction by $\boldsymbol{R}^0 = (X^0,0)$, where $X^0 = -e\mathcal{E}/(m\bar{\omega}_X^2)$ is controlled by the external electric field $\mathcal{E}$. On the other hand, Eq. (3b) contains the competition

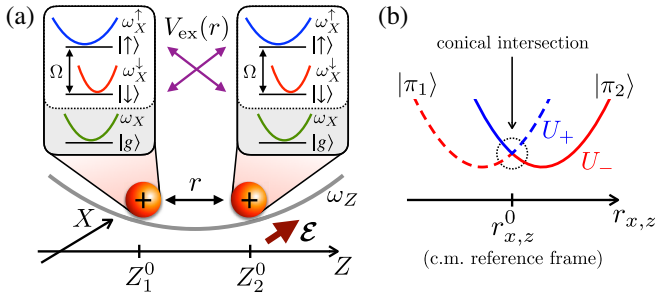

FIG. 1. Conical intersection in a system of two Rydberg ions. (a) Two ions are confined by a harmonic trapping potential in the X–Z plane. From the ground state $|g\rangle$, each ion is excited to the two Rydberg states $|\downarrow\rangle = |nS\rangle$ and $|\uparrow\rangle = |nP\rangle$. Because of different polarizabilities, ions in Rydberg states experience a state-dependent trapping potential along X, with frequencies $\omega_X^{\downarrow,\uparrow}$, and different equilibrium positions. When excited to the pair states $|\pi_1\rangle = |\uparrow\downarrow\rangle$ and $|\pi_2\rangle = |\downarrow\uparrow\rangle$, ions interact through the exchange interaction $V_{\rm ex}$, whose strength depends on their separation r. A static offset electric field $\boldsymbol{\mathcal{E}}$ allows us to control the transverse equilibrium position of the ions. (b) The interplay between the exchange interaction and the state-dependent confinement shifts the energies of the states $|\pi_1\rangle$ (dashed curve) and $|\pi_2\rangle$ (solid curve). This results in a conical intersection in the potential energy surfaces U_- (red) and U_+ (blue) which, in the reference frame of the center of mass of the system, occurs at the ions' relative equilibrium separation $r_{x,z}^0$. See text for details.

between the harmonic potential and the repulsive Coulomb interaction. Finally, the last term in Eq. (2b) is given by $H_{\mathrm{c.m.-rel}} = A^2\rho_- Xx \otimes S_z$ and describes the coupling between the electronic and nuclear motion arising from the unequal polarizabilities of the Rydberg states.

For typical experimental values, the Coulomb repulsion represents the largest energy scale of the system associated with mechanical motion. Therefore, to investigate its dynamics, one can treat H^1_{spin} as a small perturbation to H^0_{spin} [48]. We first perform a harmonic approximation around the unperturbed equilibrium positions of the ions, $\boldsymbol{R}^0$ and $\boldsymbol{r}^0$, by introducing the displacements $\boldsymbol{Q} = \boldsymbol{R} - \boldsymbol{R}^0$ and $\boldsymbol{q} = \boldsymbol{r} - \boldsymbol{r}^0$. Here, $\boldsymbol{R}^0$ and $\boldsymbol{r}^0$ are determined by Eq. (3). In particular, $\boldsymbol{r}^0 = (0, z^0)$, where $x^0 = 0$ due to symmetry considerations and z^0 is given by the solution of $\partial_z V_{\mathrm{rel}}|_{z=z_0} = 0$. We can then expand H^1_{spin} to the first order in the displacements $\boldsymbol{Q}$ and $\boldsymbol{q}$ and obtain the full spin Hamiltonian H_{spin} in the harmonic approximation. An examination of the various contributions to Eq. (2a) suggests that the most interesting part of the dynamics occurs in the relative coordinate sector, as we show in the Supplemental Material [49]. By neglecting the motion of the c.m. (i.e., by setting $\boldsymbol{Q} = \boldsymbol{0}$), and focusing exclusively on the relative coordinate $\boldsymbol{q}$, we finally obtain

$$H_{\mathrm{spin}} \approx S(\boldsymbol{q}) \otimes S_0 + G(\boldsymbol{q}) \otimes S_z + W(\boldsymbol{q}) \otimes S_x, \quad (4)$$

where $S(\boldsymbol{q}) = \mu \boldsymbol{q}^T \mathcal{K}^q \boldsymbol{q}/2$, and

$$G(\boldsymbol{q}) = A^2\rho_- X^0 q_x, \quad (5a)$$

$$W(\boldsymbol{q}) = V^0_{\mathrm{ex}} + F^0_z q_z. \quad (5b)$$

Here, we have introduced the dynamical matrix $\mathcal{K}^q_{\alpha\beta} = \mu^{-1}\partial_{r_\alpha, r_\beta} V_{\mathrm{rel}}|_{\boldsymbol{R}^0, \boldsymbol{r}^0}$, with $\alpha, \beta \in \{x, z\}$, defined $V^0_{\mathrm{ex}} = V_{\mathrm{ex}}(r^0)$, and denoted with F^0_z the z component of $\nabla_{\boldsymbol{r}} V_{\mathrm{ex}}(r)|_{\boldsymbol{r}=\boldsymbol{r}^0}$.

In the Hamiltonian of Eq. (4) one can recognize the minimal model which can host a CI [2,19]. This represents the main result of our work and shows that a CI can be actually realized in an experimentally feasible system of two trapped Rydberg ions. The high degree of control on both electronic and vibrational degrees of freedom makes this platform an ideal candidate for the study of the coherent dynamics occurring in neighborhood of a CI, as we will show in the next sections.

CI-induced dynamics in the nuclear motion.—In the spirit of the Born-Huang approach [50], the nuclear motion of the ions is determined by the PESs. The latter are given by the eigenvalues of the electronic Hamiltonian H_{spin},

$$U_\pm(\boldsymbol{q}) = S(\boldsymbol{q}) \pm \sqrt{[G(\boldsymbol{q})]^2 + [W(\boldsymbol{q})]^2}. \quad (6)$$

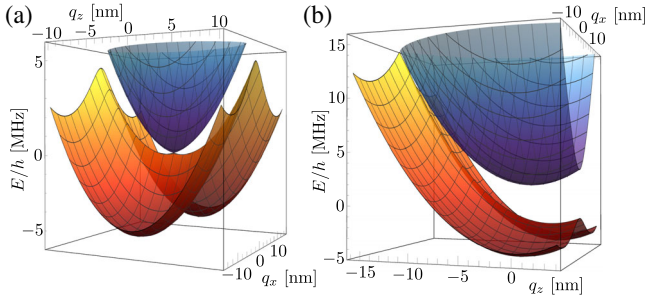

FIG. 2. Potential energy surfaces in the branching plane. Plot of the eigenvalues of Eq. (4) (i.e., the PESs) $U_\pm(\boldsymbol{q})$ as a function of the displacements q_x and q_z. (a) For $V^0_{\mathrm{ex}}/h = 0$, a CI occurs at $\boldsymbol{q}^* = (0, 0)$ while for (b) $V^0_{\mathrm{ex}}/h = 2\pi \times 0.3$ MHz the CI is shifted to $\boldsymbol{q}^* = (0, -V^0_{\mathrm{ex}}/F^0_z)$ (see text for details). Here, we considered $^{88}\mathrm{Sr}^+$ Rydberg ions, with $m = 87.9 \times 1.66 \times 10^{-27}$ kg, and set $\omega_X = 2\pi \times 1.6$ MHz, $\omega_Z = 2\pi$ MHz, $\mathcal{E} = 2.529$ V/m (resulting in $X^0 = -0.024$ μm), $\rho_\downarrow = 8.9 \times 10^{-31}$ C^{2}m^2/J, $\rho_\uparrow = -3.8 \times 10^{-30}$ C^{2}m^2/J (corresponding to Rydberg $|nS\rangle$ and $|nP\rangle$ states with $n = 50$), and $F^0_z/h = 2\pi \times 20$ MHz/μm.

In general, CIs arise at positions $\boldsymbol{q}^*$ such that $U_+(\boldsymbol{q}^*) = U_-(\boldsymbol{q}^*)$. From Eq. (6) this is equivalent to $G(\boldsymbol{q}^*) = W(\boldsymbol{q}^*) = 0$, which implies that the system described by Eq. (4) has a CI at $q^*_x = 0$ and $q^*_z = -V^0_{\mathrm{ex}}/F^0_z$. Two examples of the PESs in the neighborhood of the latter are shown in Fig. 2 for different values of V^0_{ex}.

The eigenstates associated with the PESs $U_\pm(\boldsymbol{q})$, which define the electronic *adiabatic basis*, are [30,31]

$$|\varphi_+(\boldsymbol{q})\rangle = \cos[\Lambda(\boldsymbol{q})]|\pi_1\rangle + \sin[\Lambda(\boldsymbol{q})]|\pi_2\rangle, \quad (7a)$$

$$|\varphi_-(\boldsymbol{q})\rangle = -\sin[\Lambda(\boldsymbol{q})]|\pi_1\rangle + \cos[\Lambda(\boldsymbol{q})]|\pi_2\rangle, \quad (7b)$$

where $\Lambda(\boldsymbol{q})$ is fixed by $\tan[2\Lambda(\boldsymbol{q})] = W(\boldsymbol{q})/G(\boldsymbol{q})$. Note that if $\boldsymbol{q}$ is varied along a close path encircling the CI, the mixing angle $\Lambda(\boldsymbol{q})$ changes only by π instead of 2π: the states $|\varphi_\pm(\boldsymbol{q})\rangle$ acquire an extra phase of π, known as the GP [14,15,19].

For the sake of simplicity, we first consider a suitably tailored exchange interaction potential such that $V^0_{\mathrm{ex}} = 0$ [40,49]. In this case, the CI occurs at $\boldsymbol{q}^* = \boldsymbol{0}$ and the PESs, shown in Fig. 2(a), are symmetric under the reflections $\boldsymbol{q} \to -\boldsymbol{q}$. As a consequence, the two paths connecting the two minima of $U_-(\boldsymbol{q})$ and encircling the CI from opposite sides are identical. This represents the ideal setting to investigate dynamical effects induced by the presence of a CI and, in particular, those related to the GP.

To do so, we first initialize the system's nuclear wave function in the state $\phi^{\mathrm{ss}}_{\mathrm{rel}}(\boldsymbol{q})$, corresponding to a Gaussian centered around $(q^0_{x,\mathrm{ss}}, 0)$ [49]. Here, we set $q^0_{x,\mathrm{ss}}$ to coincide with one of the two minima of $U_-(\boldsymbol{q})$ [see Fig. 2(a)]. As explained in the Supplemental Material [49], this allows us

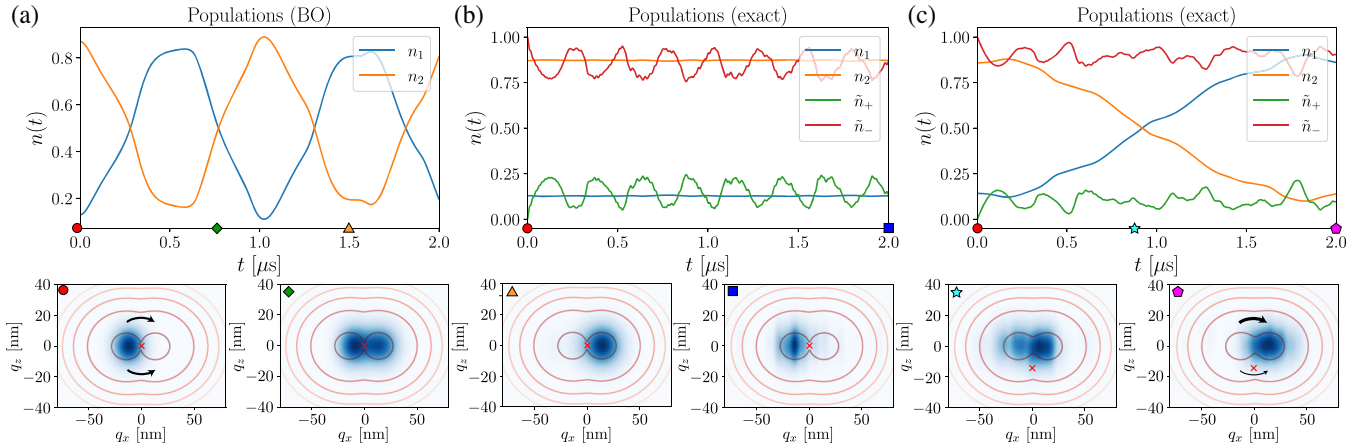

FIG. 3. Dynamics of the diabatic and adiabatic populations. Time evolution of the populations $n_k(t)$ of the diabatic states $|\pi_1\rangle$ (blue curve) and $|\pi_2\rangle$ (yellow curve) in the (a) BO approximation, (b) exact dynamics with $V^0_{\rm ex}/h = 0$, and (c) exact dynamics with $V^0_{\rm ex}/h = 2\pi \times 0.3$ MHz. In (b),(c), the populations of the adiabatic states, $\tilde{n}_-(t)$ (red curves) and $\tilde{n}_+(t)$ (green curves) are also shown. (b) The complete destructive interference between the two paths surrounding the CI results in the freezing of the nuclear motion in the c.m. reference frame. (c) A finite $V^0_{\rm ex}$ shifts the CI and breaks the perfect symmetry between the two paths observed in (b). As a consequence, the nuclear wave packet can move to the other local minimum of $U_-(\boldsymbol{q})$ and the diabatic populations $n_k(t)$ swap with each other. The bottom row illustrates some snapshots of the dynamics of the nuclear density $\mathcal{N}(\boldsymbol{q}, t)$ in the c.m. reference frame associated with the various time evolutions shown in the upper row (see the corresponding marks). Here, red contours display the behavior of $U_-(\boldsymbol{q})$, with lighter tones corresponding to larger values, while the cross highlights the position of the CI. The arrows in the first and last plots are a sketch of the weight of the nuclear wave packets encircling the opposite sides of the CI. In all panels, the system is initialized in the state $|\psi_0(\boldsymbol{q})\rangle$, with $q^0_{x,\rm ss} = -0.011$ μm. Other parameters are as in Fig. 2.

to maximize the visibility of the GP effects thanks to symmetries of the system. Then, to initiate the dynamics in the spin subspace $\mathcal{H}_{\rm sp}$, we temporarily turn on a MW field coupling the $|\downarrow\rangle$ and $|\uparrow\rangle$ states (see Fig. 1) in such a way that the electronic state is fully transferred to the lower PES eigenstate $|\varphi_-(\boldsymbol{q})\rangle$. After that, the MW field is turned off. The subsequent dynamics in the subspace $\mathcal{H}_{\rm sp}$ is then governed by $H_{\rm rel} = -\nabla^2_{\boldsymbol{q}}/(2\mu) \otimes S_0 + H_{\rm spin}$ [see Eqs. (4) and (5)], with the initial state given by $|\psi_0(\boldsymbol{q})\rangle = |\psi(\boldsymbol{q}, t = 0)\rangle = \phi^{\rm ss}_{\rm rel}(\boldsymbol{q})|\varphi_-(\boldsymbol{q})\rangle$.

We now inspect the time evolution of the populations of the two PESs, $\tilde{n}_\mu(t)$, and of the diabatic basis states, $n_k(t)$. These can be obtained by expanding the full time-dependent wave function as

$$|\psi(\boldsymbol{q}, t)\rangle = \sum_{k=1,2} \phi_k(\boldsymbol{q}, t)|\pi_k\rangle = \sum_{\mu=\pm} \tilde{\phi}_\mu(\boldsymbol{q}, t)|\varphi_\mu(\boldsymbol{q})\rangle, \qquad (8)$$

where the coefficients $\phi_k(\boldsymbol{q}, t)$ $[\tilde{\phi}_\mu(\boldsymbol{q}, t)]$ represent the diabatic (adiabatic) nuclear wave function components. Hence, the populations of the diabatic and adiabatic states are given by $n_k(t) = \int |\phi_k(\boldsymbol{q}, t)|^2 d^2\boldsymbol{q}$ and $\tilde{n}_\mu(t) = \int |\tilde{\phi}_\mu(\boldsymbol{q}, t)|^2 d^2\boldsymbol{q}$, respectively.

To identify the effects induced by the CI, we compare the exact dynamics of the system, which takes into account the presence of the two crossing PESs, with a BO approximation, in which the nuclear motion takes place on the lower PES only. In both cases, the nuclear dynamics is obtained by solving numerically the time-dependent Schrödinger equation associated with $H_{\rm rel}$ in the diabatic representation via a Crank-Nicholson scheme [49,51].

In the BO approximation, the nuclei oscillate around the equilibrium position $\boldsymbol{r}^0$ of the relative motion and in the c.m. reference frame the nuclear density $\mathcal{N}(\boldsymbol{q}, t) = \sum_k |\phi_k(\boldsymbol{q}, t)|^2$ moves from one minimum of $U_-(\boldsymbol{q})$ to the other. The effects of this motion can be directly observed in the time evolution of the diabatic populations $n_k(t)$, which can be monitored in real time via a spectroscopic measurement of the Rydberg states. As shown in Fig. 3(a), the oscillatory motion of the nuclear density gives rise to large oscillations in $n_k(t)$. This changes drastically when the exact dynamics in the presence of the CI at $\boldsymbol{q}^* = \boldsymbol{0}$ is considered. Because of the symmetry of the PESs, in moving from one minimum of $U_-(\boldsymbol{q})$ to the other, the nuclear wave packet splits evenly on the two paths encircling the CI on the opposite sides. The relative GP accumulated in this motion around the CI on the two paths differs by π and results in a perfect destructive interference at the other minimum of $U_-(\boldsymbol{q})$. As a consequence, the nuclei are inhibited from moving: the nuclear density $\mathcal{N}(\boldsymbol{q}, t)$ is stuck in the initial minimum of $U_-(\boldsymbol{q})$. This has direct impact on the diabatic populations, shown in Fig. 3(b), which exhibit only small oscillations around their initial values.

To confirm that the observed behavior is entirely due to the GP, we have also considered a BO approximation in which the diagonal BO correction terms have also been

included. The latter take into account the additional potential energy barrier induced by the presence of the CI [19,52]. As shown in the Supplemental Material [49], the inclusion of the diagonal BO correction does not prevent the oscillatory dynamics of the nuclei (and of diabatic populations) but only results in a slight increase of the period of the oscillations.

Controlling the CI.—So far we considered the case in which the CI is located at the saddle point of $U_-(\boldsymbol{q})$ and the PESs are highly symmetric around the CI. This was achieved with a fine-tuned exchange interaction potential, such that $V_{\mathrm{ex}}^0 = 0$. We now examine the more general case with $V_{\mathrm{ex}}^0 \neq 0$. This leads to a scenario common to many real molecules, in which CIs are located on the slope of (asymmetric) PESs [53–55]. As shown in Eq. (5b), a finite value of V_{ex}^0 allows one to control the coordinate q_z^* of the CI. In this case, the symmetry of the PESs around the CI is broken and the paths encircling the two sides of the CI are no longer equivalent [Fig. 2(b)]. This provides a clear demonstration of the fact that the freezing of the nuclear motion is due to a perfect destructive interference caused by a GP. Indeed, when $V_{\mathrm{ex}}^0 \neq 0$, the initial nuclear wave function splits in two wave packets with different weights and the interference between the two paths encircling the CI occurs only partially. As a consequence, the nuclear density $\mathcal{N}(\boldsymbol{q}, t)$ can now move from one minimum of $U_-(\boldsymbol{q})$ to the other and the time evolution of the diabatic populations differs significantly from the one of Fig. 3(b): as shown in Fig. 3(c), $n_1(t)$ and $n_2(t)$ oscillate and swap with each other after a time interval proportional to V_{ex}^0.

More complex scenarios can be obtained by considering systems with more than two ions. For instance, in the Supplemental Material we show that our approach can be readily generalized to a three-ion setup [49]. This provides a flexible experimental platform to study the full quantum dynamics of CIs involving more than two PESs, whose numerical investigation would require a huge amount of computational resources.

Conclusions.—We have demonstrated that a minimal setup of two trapped Rydberg ions can be exploited to engineer a CI in a highly tunable system. An external static electric field and a tailored exchange interaction potential between Rydberg states fully control the shape of the two crossing PESs and the location of the CI. The high degree of control on the electronic and vibrational states of the ions makes it possible to simulate the dynamics of a wave packet around the CI. We have shown that interference effects due to the GP near a CI inhibit the movement of nuclear wave packets. This phenomenon has a direct impact on the populations of the Rydberg states and can thus be readily observed through a spectroscopic measurement. Extending this study to many-ion systems would make it possible to analyze the dynamics near CIs in more complex environments, such as in the presence of dissipation induced by coupling to many phonon modes [44–46].

The authors would like to thank S. Wüster for useful discussions. The research leading to these results has received funding from the EPSRC Grant No. EP/M014266/1, the EPSRC Grant No. EP/R04340X/1 via the QuantERA project "ERyQSenS," and the Deutsche Forschungsgemeinschaft (DFG) within the SPP 1929 Giant interactions in Rydberg Systems (GiRyd) under Project No. 428276754. C. Z. and M. H. acknowledge support from the Swedish Research Council (TRIQS), the QuantERA ERA-NET Cofund in Quantum Technologies (ERyQSenS), and the Knut & Alice Wallenberg Foundation (WACQT). C. Z. acknowledges the hospitality of the University of Nottingham. I. L. acknowledges funding from the "Wissenschaftler Rückkehrprogramm GSO/CZS" of the Carl-Zeiss-Stiftung and the German Scholars Organization e.V. W. L. acknowledges funding from the UKIERI-UGC Thematic Partnership No. IND/CONT/G/16-17/73, and the Royal Society through the International Exchanges Cost Share Grant No. IEC\NSFC\181078.

[1] M. Born and R. Oppenheimer, Ann. Phys. (N.Y.) **389**, 457 (1927).
[2] W. Domcke, D. R. Yarkony, and H. Köppel, *Conical Intersections. Electronic structure, Dynamics and Spectroscopy* (Word Scientific, Singapore, 2004).
[3] J. C. Tully, J. Chem. Phys. **137**, 22A301 (2012).
[4] D. R. Yarkony, Rev. Mod. Phys. **68**, 985 (1996).
[5] M. Baer, *Beyond Born-Oppenheimer. Conical Intersections and Electronic Nonadiabatic Coupling Terms* (Wiley-Interscience, Hoboken, 2006).
[6] N. Ismail, L. Blancafort, M. Olivucci, B. Kohler, and M. A. Robb, J. Am. Chem. Soc. **124**, 6818 (2002).
[7] S. Perun, A. L. Sobolewski, and W. Domcke, J. Am. Chem. Soc. **127**, 6257 (2005).
[8] M. Barbatti, A. J. A. Aquino, J. J. Szymczak, D. Nachtigallová, P. Hobza, and H. Lischka, Proc. Natl. Acad. Sci. U.S.A. **107**, 21453 (2010).
[9] R. Schoenlein, L. Peteanu, R. Mathies, and C. Shank, Science **254**, 412 (1991).
[10] D. Polli, P. Altoè, O. Weingart, K. M. Spillane, C. Manzoni, D. Brida, G. Tomasello, G. Orlandi, P. Kukura, R. A. Mathies, M. Garavelli, and G. Cerullo, Nature (London) **467**, 440 (2010).
[11] S. Rinaldi, F. Melaccio, S. Gozem, F. Fanelli, and M. Olivucci, Proc. Natl. Acad. Sci. U.S.A. **111**, 1714 (2014).
[12] L. Hammarström and S. Styring, Phil. Trans. R. Soc. B **363**, 1283 (2008).
[13] A. Bohm, A. Mostafazadeh, H. Koizumi, Q. Niu, and J. Zwanziger, *The Geometric Phase in Quantum Systems* (Springer-Verlag, Berlin, 2003).
[14] H. C. Longuet-Higgins, U. Öpik, M. H. L. Pryce, and R. A. Sack, Proc. R. Soc. A **244**, 1 (1958).
[15] M. V. Berry, Proc. R. Soc. A **392**, 45 (1984).
[16] C. A. Mead, Rev. Mod. Phys. **64**, 51 (1992).
[17] S. C. Althorpe, T. Stecher, and F. Bouakline, J. Chem. Phys. **129**, 214117 (2008).

[18] I. G. Ryabinkin and A. F. Izmaylov, Phys. Rev. Lett. **111**, 220406 (2013).

[19] I. G. Ryabinkin, L. Joubert-Doriol, and A. F. Izmaylov, Acc. Chem. Res. **50**, 1785 (2017).

[20] H.-D. Meyer, F. Gatti, and G. A. Worth, *Multidimensional Quantum Dynamics.* (Wiley-VCH, Weinheim, 2009).

[21] A. D. G. Nunn, R. S. Minns, R. Spesyvtsev, M. J. Bearpark, M. A. Robb, and H. H. Fielding, Phys. Chem. Chem. Phys. **12**, 15751 (2010).

[22] M. Kowalewski, K. Bennett, K. E. Dorfman, and S. Mukamel, Phys. Rev. Lett. **115**, 193003 (2015).

[23] S. Adachi, T. Schatteburg, A. Humeniuk, R. Mitrić, and T. Suzuki, Phys. Chem. Chem. Phys. **21**, 13902 (2019).

[24] L. Young *et al.*, J. Phys. B **51**, 032003 (2018).

[25] M. Šindelka, N. Moiseyev, and L. S. Cederbaum, J. Phys. B **44**, 045603 (2011).

[26] N. Moiseyev, M. Šindelka, and L. S. Cederbaum, J. Phys. B **41**, 221001 (2008).

[27] A. O. G. Wallis, S. A. Gardiner, and J. M. Hutson, Phys. Rev. Lett. **103**, 083201 (2009).

[28] T. F. Gallagher, *Rydberg Atoms* (Cambridge University Press, New York, 2005).

[29] R. Löw, H. Weimer, J. Nipper, J. B. Balewski, B. Butscher, H. P. Büchler, and T. Pfau, J. Phys. B **45**, 113001 (2012).

[30] S. Wüster, A. Eisfeld, and J. M. Rost, Phys. Rev. Lett. **106**, 153002 (2011).

[31] S. Wüster and J.-M. Rost, J. Phys. B **51**, 032001 (2018).

[32] M. Müller, L. Liang, I. Lesanovsky, and P. Zoller, New J. Phys. **10**, 093009 (2008).

[33] F. Schmidt-Kaler, T. Feldker, D. Kolbe, J. Walz, M. Müller, P. Zoller, W. Li, and I. Lesanovsky, New J. Phys. **13**, 075014 (2011).

[34] W. Li and I. Lesanovsky, Phys. Rev. Lett. **108**, 023003 (2012).

[35] W. Li and I. Lesanovsky, Appl. Phys. B **114**, 37 (2014).

[36] G. Higgins, W. Li, F. Pokorny, C. Zhang, F. Kress, C. Maier, J. Haag, Q. Bodart, I. Lesanovsky, and M. Hennrich, Phys. Rev. X **7**, 021038 (2017).

[37] G. Higgins, F. Pokorny, C. Zhang, Q. Bodart, and M. Hennrich, Phys. Rev. Lett. **119**, 220501 (2017).

[38] A. Mokhberi, J. Vogel, J. Andrijauskas, P. Bachor, J. Walz, and F. Schmidt-Kaler, J. Phys. B **52**, 214001 (2019).

[39] J. Vogel, W. Li, A. Mokhberi, I. Lesanovsky, and F. Schmidt-Kaler, Phys. Rev. Lett. **123**, 153603 (2019).

[40] F. M. Gambetta, C. Zhang, M. Hennrich, I. Lesanovsky, and W. Li, Phys. Rev. Lett. **125**, 133602 (2020).

[41] C. Zhang, F. Pokorny, W. Li, G. Higgins, A. Pöschl, I. Lesanovsky, and M. Hennrich, Nature (London) **580**, 345 (2020).

[42] G. Higgins, F. Pokorny, C. Zhang, and M. Hennrich, Phys. Rev. Lett. **123**, 153602 (2019).

[43] G. Higgins, *A Single Trapped Rydberg Ion* (Springer, Cham, 2019).

[44] A. Kühl and W. Domcke, J. Chem. Phys. **116**, 263 (2002).

[45] L. Chen, M. F. Gelin, V. Y. Chernyak, W. Domcke, and Y. Zhao, Faraday Discuss. **194**, 61 (2016).

[46] R. Ulbricht, S. Dong, I.-Y. Chang, B. M. K. Mariserla, K. M. Dani, K. Hyeon-Deuk, and Z.-H. Loh, Nat. Commun. **7**, 13510 (2016).

[47] F. G. Major, V. N. Gheorghe, and G. Werth, *Charged Particle Traps*, Vol. 1 (Springer-Verlag, Berlin, 2005).

[48] This can be further confirmed by a self-consistency check. Using the parameters given later in the text, we obtain $\|H^0_{\mathrm{spin}}\|/\hbar \sim 2\pi \times 10^5$ MHz and $\|H^1_{\mathrm{spin}}\|/\hbar \sim 2\pi$ MHz, with $\|\cdot\|$ being the matrix spectral norm.

[49] See Supplemental Material at http://link.aps.org/supplemental/10.1103/PhysRevLett.126.233404 for details on the derivation of Eq. (4), the preparation of the nuclear initial state $\phi^{\mathrm{ss}}_{\mathrm{rel}}(\boldsymbol{q})$, the tailored exchange interaction potential $V_{\mathrm{ex}}(r)$, the BO approximation, and the generalization to a three-ion setup.

[50] M. Born and K. Huang, *Dynamical Theory of Crystal Lattices* (Clarendon Press, Oxford, 1954).

[51] J. W. Thomas, *Numerical Partial Differential Equations: Finite Difference Methods*, Vol. 1 (Springer-Verlag, New York, 1995).

[52] R. Gherib, L. Ye, I. G. Ryabinkin, and A. F. Izmaylov, J. Chem. Phys. **144**, 154103 (2016).

[53] B. G. Levine and T. J. Martínez, Annu. Rev. Phys. Chem. **58**, 613 (2007).

[54] J. Yang *et al.*, Science **361**, 64 (2018).

[55] K. F. Chang, M. Reduzzi, H. Wang, S. M. Poullain, Y. Kobayashi, L. Barreau, D. Prendergast, D. M. Neumark, and S. R. Leone, Nat. Commun. **11**, 4042 (2020).